Colorimetric sensing by Naphthalene-Pyridine containing unit of Schiff base ligand for multimetallic ion detection for Fe 2+ , Fe 3+ , and Cu 2+

Poonam Kaswan (poonamcym@gmail.com)
Amity University Haryana

Research Article

Keywords:

Posted Date: June 12th, 2023

DOI: https://doi.org/10.21203/rs.3.rs-3045337/v1

Abstract

A hydroxyl Schiff-base namely 2-(1-(pyridin-2-ylmethylimino)ethyl) naphthalen-1-ol (PMNOL) having naphthalene and pyridine units has been synthesized and characterized using 1H NMR, 13C NMR, FTIR and UV-vis spectroscopy. Solvent and pH has a significant impact on the UV-vis spectroscopy of PMNOL as ascertained. The UV-Visible spectra technique has been applied to evaluate the sensing capacity towards the metal ions Ni2+, Co2+, Cu2+, Fe2+, Fe3+, Hg2+, Al3+ Cr3+, Ca2+and Cd2+ in the combination of methanol and DMF. By applying the UV-Vis spectra, a considerable shift (50-120) from the origin has been reported. Azomethine (>C=N-) with hydroxyl (-OH) moieties as contained by Schiff base ligand were reported as a colorimetric chemosensor as it coordinates easily with metals and produces coloured metal complexes. The Schiff base ligand displayed colorimetric characteristics with Cu2+, Fe2+, and Fe3+ and as a consequence a distinct shift in colour for every metal can easily be recognized by the naked eye. The stoichiometric ratio 1:1 coordination complexation for PMNOL-Fe2+, PMNOL-Cu2+, and a 2:1 complex mode for HNMAP-Fe3+ by UV-visible titration as well as Job's plot were postulated. PMNOL may have sensing potential for Fe2+, Fe3+ and Cu2+ colorimetric detection effectively. The addition of ligand to the metal ions is might be because of LMCT, so as to inhibit C=N isomerization and ICT. Graphical abstract

1. Introduction

Colorimetric sensors have gradually grown in popularity because, instead of expensive equipment, colorimetric sensors were successfully used for metal ion measurement and recognition with the naked eye.[1–4] Among recognized sensors, Schiff bases were well-known chemosensors for sensing cations as well as anions.[5–9] Schiff bases has the ability to synchronize with almost every metal ion by azomethine group's N-atom and other donors atoms such as nitrogen, sulfur or oxygen atoms adjoining to the azomethine group.[14,15] Various Schiff bases were utilized as chemosensors for the detection of metal ions like Ni^{2+}, Co^{2+}, Mg^{2+}, Cu^{2+}, Fe^{2+}, Mn^{2+}, Zn^{2+}, Fe^{3+}, Hg^{2+}, Al^{3+}, Fe^{3+}, Cr^{3+}, and Pb^{2+}.[12–18] Sensors having molecular architectures containing a naphthalene, crown ether, coumarin, pyridines, quinolines and pyrene have been designed to bond with metal ions.[19–22] For this purpose, naphthalene-based chemosensors were highly prominent.[23–25] 1-hydroxy-2-acetonaphthone, phenolic Schiff ligands must provide a foundation for the synthesis of varied transition metal complexes employed in several applications[26]. As negative ramifications of transition metal ions, such as high toxicity on human health and the environment, detecting these transition metal ions as pollutants has been a primary goal in the pharmaceutical, biological, and geosciences disciplines[27–29]. Various methods identified and utilized for governing dangerous/harmful transition metal elements which includes ICP, AAS, ICPMS, and fluorescence spectroscopy[30–33]. The cost of analysis per sample is generally hefty, and all of these methods are laborious to acquire and execute. Normally, they need a complex procedure for ion analysis. As a result, research is focusing on the use of organic compounds with optical responses as chemical sensors for metal ion analysis, so that expensive and sophisticated metal detection techniques may be simply handled by easy viewing with the naked eye. Colorimetric analysis was performed to assess Schiff bases as a chemosensor for detecting heavy metal ions through visual colour changes.[11] With

great specificity and selectivity, the metal ions were sensed by the organic molecules having fluorescence and colorimetric characteristics which were synthesized with great effort.[34–39] It has been usually acknowledged that UV-vis spectra has been produced from the electronic transition from the ground to excited states of atoms and molecules.[40–45] Molecules with πe^- or non-bonding e^- absorbs UV or visible light energy and e^- get excited to upper anti-bonding MO resulting in colour variation. Naphthalene-based Schiff bases have been researched for the sensing of metals as shown in **Chart 1**.[46–49] commonly with Fe^{2+} and Fe^{3+} ions.[46–50] A probe of naphthalenol (FIMN) for Al^{3+}, Fe^{3+}, Co^{2+} and Cu^{2+} ions with detection limit 2.643×10^{-8}, 1.843×10^{-6}, 8.349×10^{-5} and 5.035×10^{-5} M respectively was examined which was elucidated by C = N isomerization.[23] Another study for Co^{2+}, $Cu^{2+}$and F^- ions for environmental purposes and addresses the attachment of biomaterials such as DNA as well as BSA.[51] A naphthalene Calix [4] arene in determining of Zr^{4+} and Fe^{2+} with LOD 1.98 nM and 4.05 nM due to LMCT.[24] Folic acid, one of the crucial B vitamins can be identified by novel fluorene-naphthalene moiety.[25] Other aniline-naphthalene dialdehyde for copper(II) ions detection has a limit of 1.64×10^{-8} mol L^{-1}.[52]

Keeping all the above details in mind, a novel NNO donor naphthalic Schiff base ligand, **PMNOL** was designed by the condensation of HAN with 2-(aminomethyl)pyridine in 1:1 ratio. The tridentate ligand supplies the metal centers with an NNO coordinated environment, and as a consequence, a stable metal complex was synthesized and UV-vis absorbance was thoroughly scrutinized and established that PMNOL may identify metal ions, Fe^{2+}, Cu^{2+} and Fe^{3+} with great selectivity utilizing a variety of steric and charge effects.

2. Experimental section

2.1. Reagents and Apparatuses –

The precursor chemicals, such as 2-aminothiophenol, 4-(dimethylamino)benzaldehyde, sulphate salts of Ni^{2+}, Co^{2+}, Mg^{2+}, Cu^{2+}, Fe^{2+}, Mn^{2+}, Zn^{2+}, Fe^{3+}, Hg^{2+}, Al^{3+} Fe^{3+}, Cr^{3+}, and Pb^{2+} and solvents such as DMF, ethyl acetate, water, methanol, hexane, cyclohexane and ethanol used for the research was of an analytical kind bought by Sigma-Aldrich and no need of purification. The UV HPLC spectroscopic grade DMF solvent used in the experiments had a purity of 99.7%. A Thermo Scientific Evolution 300 UV-Visible dual beam spectrophotometer was used to record UV-Vis absorption spectra. At room temperature, the FTIR spectra of PMNOL by KBr disc were obtained using a Nicolet NEXUS 870 FTIR spectrophotometer ranging between 4000 to 500 cm^{-1}. The ^{13}C and ^{1}H NMR spectra were acquired at 400 MHz via Bruker AMX-500 spectrometer with TMS as the reference and chloroform as the solvent. The pH value was checked using a PHS-25 pH meter.

2.2. Preparation of PMNOL

The Schiff base ligand 2-(1-(pyridin-2-ylmethylimino) ethyl) naphthalene-1-ol (**Scheme 1**) was prepared by following the reported procedure.[53] 1-hydroxy-2-acetonaphthone (1 g, 5.40 mmol) was added to a 100 mL

round bottom flask. A solution of 2-(aminomethyl) pyridine (5.55 mL, 5.40 mmol) in 40 mL of ethanol added to above solution dropwise and refluxed, for 3 hours. The solvent was evaporated, washed with cold methanol, and dried to give the Ligand as a yellow solid. The yield of the prepared ligand was found to be 82% (1.23 g). In the lab, 2-(1-(pyridin-2-ylmethylimino) ethyl) naphthalene-1-ol was produced. Ligand is characterised by FTIR (Fig. 1), NMR (Fig. 2 and Fig. 3) and mass spectra (Fig. 4).

2.3 Absorption study of PMNOL ligand by using UV-Vis spectra

The highest wavelength of UV-Visible absorption maxima (λ_{max}) for native chemosensor PMNOL was obtained in DMF just at ambient temperature in combination factor concentration of 10^{-6} to 5.0×10^{-5} M spanning the spectral region 200–800 nm (**Fig. 7**).

2.3.1. PMNOL Behaviour in polar/non-polar solvent

The solvent polarity will have a substantial influence on the UV-vis absorbance value of PMNOL. As a result, several polar solvents including DMF, ethanol, DMSO, chloroform, acetonitrile, methanol, acetonitrile, ethyl acetate, and water studied with the concentration of 5.0×10^{-5} mol·L^{-1} of **PMNOL** concentration (Fig. 6).

3.2. pH effect on absorbance value PMNOL

pH has a substantial influence on its present form as a protic sensing material, which affects its spectral characteristics. As a consequence, the influence of pH on the spectra of UV-visible of PMNOL in Methanol/DMF (v/v = 1:1) from pH 4.0 to pH 10.0 was investigated and recorded (**Fig. 7**).

2.3.3 The identification of different metal ions using colorimetry

It must have been performed at room temperature utilizing 2.5 mL of each Ni^{2+}, Co^{2+}, Cu^{2+}, Fe^{2+}, Fe^{3+}, Hg^{2+}, Al^{3+} Cr^{3+}, $Ca^{2+}$and Cd^{2+} metal ion solution (5.0×10^{-2} M) and Schiff base ligand with 2.5 mL (5.0×10^{-2} M). After then, the solution mixture was diluted to 5 mL with DMF/CH_3OH solvent. The pH of the mixture of the solution is 7.25. The spectra of UV-Visible, mixtures were obtained after adequate mixing (Fig. 5).

2.3.4. UV–Visible Titration Experiment-

Transition metal ion stock solutions (Ni^{2+}, Co^{2+}, Cu^{2+}, Fe^{2+}, Fe^{3+}, Hg^{2+}, Al^{3+} Cr^{3+}, $Ca^{2+}$and Cd^{2+}) got primed including a 5×10^{-6} M concentration of sulfates of metal in methanol. The Schiff base ligand **PMNOL** chemosensor solution was produced at an increased concentration of 5×10^{-5} M and the pH of the solution was 7.25 in DMF. **PMNOL** has the benefit of being dissolved with DMF solvent (miscible with methanol). For the color change analysis, UV-Visible readings were acquired in the 200–800 nm

wavelength range, and the 300 UV-Vis dual beam spectrophotometer had a 1 cm path length as well as a quartz cell (Fig. 8).

2.3.5. Job Plot Quantification

Metallic ions solution of Cu^{2+}, $Fe^{2+,}$ and Fe^{3+} (5×10^{-5} M) as well as the ligand solution (5×10^{-5} M), are used for stoichiometry determination. A certain level of metal ions (2.5 mL) was introduced to the cuvette, followed by an increment volume of the ligand **PMNOL**. the mole fraction of ligand solution ([L]/[M] + [L]) raised by 0.1 to 0.9. The maximal intensity of absorbance at a certain wavelength was tracked and measured. for each metal Cu^{2+}, $Fe^{2+,}$ and Fe^{3+} (Fig. 9).

3. Results and Discussion

The objective of the investigation is to create coordination sites for ligands with binding capacity and effectively identify certain Aqueous transition metal cations environments using host-guest relationship mediated by metal-ligand coordination. The Schiff base compound was used as the ligand in this study. named 2-(1-(pyridin-2-ylmethylimino) ethyl) naphthalen-1-ol(**PMNOL**). The azomethine component is situated on the ortho position, the structural components of both CH = N- (azomethine) group and also the-OH(hydroxyl) component are present. This molecule is classified as a tridentate ligand because the nitrogen atom presented on the azomethine group and pyridine indeed with the hydroxyl group's oxygen ion can interact with metal cations.

3.1. Schiff Base Detector Chemical Preparation

The Schiff base ligand **PMNOL** was produced utilizing the amine 2-aminothiophenol and condensed in a molar ratio of 1:1 with the aldehyde 4-(dimethylamino)benzaldehyde molecule according to the reported procedure as shown by **Scheme 1**. Recrystallization was used to purify the produced **PMNOL** chemical, and the yield was high. It was a yellow solid that was soluble in polar solvent as ethanol, methanol DMF, chloroform, ethyl acetate, and DMSO. The cleanliness of the substances was determined by using TLC and their structural features were determined by NMR, UV-Vis, IR, CHN analysis, and mass spectra. The elemental analysis agreed well Considering the theoretically predicted percentage values for the chemical formulae given, confirming and proving the proposed tentative structures of the synthesized Schiff base ligand **PMNOL**. Furthermore, the IR spectra revealed the typical bands of azomethine (1606 cm^{-1}) and hydroxyl groups (3052 cm^{-1}). As a result, before proceeding with the sensing experiments, the PMNOL ligand structure was validated. Schiff base ligands are widely recognized to be good sensors for both cations and anions.[36,51,54–57]

FT-IR (microscope, cm^{-1}) max: 1060 (w, C-O). 1461 (m, CH_2) (s, C = C), 1530 (m),), 1606 (s, C = N), 3052 (w, O-H) as it is presented in Fig. 1

UV-vis (MeOH, 5×10^{-5} M), λmax/nm: 225(70,000), 272(82,000), 411(34,000)

^{1}H NMR (400 MHz, $CDCl_3$, δ/ppm): 14.2 (s, 1H, -OH), 8.60–8.61 (d, *J* = 4.4 Hz, 1H, H_1), 8.51–8.53 (d, *J* = 8.8, H_2), 7.67–7.70 (td, *J* = 3.4 Hz, H_6) 7.58–7.60 (d, *J* = 8.6, H_7), 7.50–7.53 (td, *J* = 3.4 Hz, H_5), 7.36–7.42 (m, 2H, H_{15}, H_{16}), 7.31–7.33 (d, *J* = 78.8 Hz, H_{17}), 7.20–7.23 (t, 1H, H_{14}), 6.81–6.83 (d, *J* = 9.5, H_4), 4.89–4.90 (s, 2H, H_{12}), 2.50 (s, 3H, H_{18})

^{13}C {^{1}H} NMR (125.7 MHz, CDCl3, δ/ppm): 177.22 (C_{11},C_{13}), 172.95 (C_9), 151.12 (C_{13}), 138.73(C_{17}), 138.22(C_8), 131.78(C_{10}), 131.05(C_1), 128.31(C_7), 126.97(C_2), 126.10(C_3), 126.15(C_4), 124.09(C_{14}), 122.76(C_{16}), 115.05(C_6), 110.23(C_5), 51.13(C_{12}), 14.02(C_{18}).

Mass spectra

Mass specta is shown here according to its molecular mass 277 as shown in Fig. 4. No any fragmentation is shown there it show the stability of sensor compound.

3.2. Colorimetry identification of Transition Metal Ions

The naked eye inspection experiment was used to assess the detection capabilities of PMNOL((5× 10^{-2} M, DMF prepared) approaching different metallic ions of Ni^{2+}, Co^{2+}, Cu^{2+}, Fe^{2+}, Fe^{3+}, Hg^{2+}, Al^{3+} Cr^{3+}, $Ca^{2+}$and Cd^{2+}. As a result in methanol, metal ion solution(5× 10^{-5} M) was introduced with increment to the solution of **PMNOL**, it appears the change in coloration from bright yellow to sea green and blackish green for Fe^{2+} and Fe^{3+}, and sea-green for Cu^{2+}, as it is shown in Fig. 5.

This investigation suggests that three metal ions effectively form metal complexes with ligand PMNOL, perhaps may via a moiety of azomethine and hydroxyl groups situated adjacent resulting from a significant affinity for these metal ions The addition of Ni^{2+}, Co^{2+}, Hg^{2+}, Al^{3+} Cr^{3+}, $Ca^{2+}$and Cd^{2+} to that same PMNOL impacting no appreciable change of color is observed. This could be attributed to the fact that Gibb's free energy to form a metal-ligand complex to all and each metal is inadequate to randomization and interaction and thus observed no impact on the metal-ligand complex formation as well as not any colors could be observed. As a result, **PMNOL** only could detect Cu^{2+}, Fe^{2+}, and Fe^{3+} ions in methanol solutions by producing a distinct coloration.

3.3. UV–Visible Monitoring

3.3.1 Solvent effect –

PMNOL displayed substantially the same spectral profile and wavelength, but with changing maximum absorption peak (A_{max}), which might be ascribed to strong delocalization of electron transit between ground and excited states. Because of their polarity and protic properties, In protic liquids including ethanol or water, the wavelength increases with increasing molar absorption coefficient (Amax), which may induce **PMNOL** in intramolecular distribution (Fig. 6). In consequence of the strong coupling of intermolecular hydrogen bonds, **PMNOL** molecules will cluster in non-protic solvents, bending the basic conjugated core or, to some extent, reducing the conjugated electron density. As a result, absorption

decreases in non-polar solvents while increasing in polar liquids. As a result, the Methanol/DMF (v/v = 1:1) mixed solvent was chosen. Because of adequate absorption in addition both metal and ligand are soluble in each other in this partivluar solvent system.

3.3.2 pH effect-

At neutral pH the absorbance is constant, with a double-peak spectral profile of UV-vis at 417 nm, demonstrating that **PMNOL** has a stable structure under neutral or acidic conditions. Absorbance increment might have formed as a result of the hydroxyl (O) in **PMNOL** molecules progressively converting to the phenolic anion, resulting in an expanded conjugated framework All subsequent studies will be conducted at pH 8 as illustrated by **Fig. 7**. The behavior of the ligand **PMNOL** for chemosensing was investigated by analyzing absorbance by the UV-Visible spectrum after introducing it to various metal ions for examination by Methanol-DMF (1:1) mixture mostly at normal temperature (Fig. 8).

3.3.3 Titration experiment –

Next, we observed the UV-Visible spectrum of the pure ligand **PMNOL** without the addition of metal in DMF, which showed absorbance at a wavelength of 421 nm broadband spectrum (Fig. 8), that we linked to the n→π* transition of a moiety of azomethine. Although the absorbance intensity of **PMNOL** at 421 nm decreased after adding Cu^{2+}, $Fe^{2+,}$ and Fe^{3+} metallic solutions to the **PMNOL** ligand, a λ_{max} shifting was detected, in the meantime, high peaks emerged at 364, 447, and 464 nm well after continuous addition of Cu^{2+}, Fe^{2+} and Fe^{3+} metallic solutions to the **PMNOL** solution, respectively. This behavior of bathochromic change might be understood by LMCT. Complexation leads the ligand **PMNOL** and metal ions causing the formation of additional band spectra[16].

The azomethine moiety strengthens the ligand's withdrawing character, resulting in more Intramolecular charge exchange first from the complex's electron-don ating group (-OH) to the metal ions. Charge density from ligand molecular orbitals to partially filled metallic d-orbitals improves metal ion reduction. The difference in a red shift among various metals might be due to differences in metal ion size as well as charge distribution. [58] The UV-Vis absorption spectra of ligand **PMNOL** did not change for those other ions because no complexation happened in these instances.

Upon incremental addition of $CuSO_4$ (5×10^{-5} M) to the solution of sensor ligand (5×10^{-5} M) in CH_3OH-DMF (1:1, v/v), there was a gradual decrease in the intensity in the region 370–420 nm. The ligand showed absorption band at 285 and 295 nm attributing to π-π* transition. The band at 275 nm successively decreased with the addition of copper salt. The equilibrium between sensor and Cu complex was indicated by the observation of three isosbestic points at 297, 305 and 396 nm, respectively. At 411-421nm, the ligand features a shoulder peak that progressively converts to a single peak and diminishes with metal ion concentration (Fig. 9). The binding constant was found to be 0.64×10^5 M^{-1} (Fig. 11). The Job's plot analysis revealed 1:1 stoichiometry (Fig. 10). Upon incremental addition of $FeSO_4$ (5×10^{-5} M) to the solution of sensor ligand (5×10^{-5} M) in CH_3OH-DMF (1:1, v/v), there was a gradual decrease in the intensity in the region 390–420 nm. The band at 275 nm successively decreased with the addition of

Fe^{2+} salt. At 411-421nm, the ligand features a shoulder peak that progressively converts to a single peak and diminishes with metal ion concentration. The equilibrium between sensor and Cu complex was indicated by the observation of three isosbestic points at 297, 305 and 396 nm, respectively (Fig. 9). The binding constant was found to be .64 × 10^5 M^{-1} (Fig. 11). The Job's plot analysis revealed 1:1 stoichiometry (Fig. 10). The ligand showed absorption band at 285 and 295 nm attributing to π-π* transition.. Upon incremental addition of $Fe_2(SO_4)_3$ (5 × 10^{-5} M) to the solution of sensor ligand (5 × 10^{-5} M) in CH_3OH-DMF (1:1,v/v), there was a gradual decrease in the intensity in the region 390–420 nm. The ligand showed absorption band at 285 and 295 nm attributing to π-π* transition. The band at 355 nm successively increased with the addition of Fe^{3+}. The equilibrium between sensor and Fe^{3+} complex was indicated by the observation of three isosbestic points at 318 and 376 nm, respectively. At 411-421nm, the ligand features a shoulder peak that progressively converts to a single peak and diminishes with metal ion concentration as shown in Fig. 9. The binding constant was found to be 0.35 × 10^5 M^{-1} (Fig. 11). The Job's plot analysis revealed 1:2 stoichiometry (Fig. 10).

The limit of detection is determined by the calibration curve Fig. 9 by the formula

LOD = 3σ/m: LOQ = 10 σ/m

Where σ = SD of intercept of the calibration curve and

m = Slope of the calibration curve

3.3.4. The stoichiometry determination by Job’s Plot

Titration studies in DMF-Methanol solution were performed to investigate the stoichiometry of metal and ligand as well as the binding process. The Job's plot with a continuous variation technique was used to calculate the ligand PMNOL's relative affinity ratio to metal cations Cu^{2+}, $Fe^{2+,}$ and Fe^{3+} for the metal complex formation (Fig. 10).[59–61]

The approach held the maximum uptake capacity of ligand **PMNOL** and different metal ions at (10^{-5} M) with changing the metal ion mole fraction ranges by 0.1 to 1.0 M. Figure 10 shows that the greatest differences in absorbance were recorded for Fe^{2+}, Cu^{2+} when the metal and ligand molar fraction was 0.50, revealing of development of a 1:1 between Metal and Ligand and for Fe^{3+} it was .70 that indicate 1:2 stoichiometry between metal and ligand. The interaction of said N-atom (azomethine moiety) and the O-atom (hydroxyl group) is one Proposed receptor - binding pattern with metal ions so it is considered PMNOL as a tridentate ligand that forms complexes of metal with the likely structure depicted in the **Chart 2**.

3.5. Binding constant

The binding constant of tridentate ligan**d PMNOL** is determined by the Benesi-Hildebrand plot (Fig. 11) between $1/[A]_0$-[A] and 1/ [Conc. of metal]. It determines the stability of complexes formed during the

titration experiment. With Cu^{2+}, Fe^{2+}, Fe^{3+} metal, and ligand-PMNOL.

4. Sensing Mechanism

The titration study via UV-visible spectral profile clarifies the recognition process of PMNOL to Fe^{2+} Fe^{3+} or Cu^{2+}, as shown in Fig. 9. The absorbance intensities at 421, 423, and 425 progressively decline with the addition of Fe^{2+}, Cu^{2+}, and Fe^{3+}. Some discrete isosbestic points found throughout the receptor-donor titration process imply the stable formed complex with a perfect ratio. The absorption intensity would be at its lowest at 1.0 equiv. of ligand for Cu^{2+}, Fe^{2+} and 2.0 equiv. of ligand for Fe^{3+}, suggested the stoichiometry ratio of complex 1:1 and 1:2 respectively. Cis-trans isomerization around the C = N bond results in the creation of a stiff five-membered metallacycle as well as an H-bonded scaffolding, leading to an ICT enhancement of the system. Due to complexation, it is observed that ICT disappears leading to strong LMCT as shown in Scheme 2.

Due of the space-size effect, Fe^{2+} and Cu^{2+} may be coordinated with both N and O atoms simultaneously to form stable 6-membered and 4-membered rings. The enhanced stiffness and planar conjugated structure will result in red-shifted absorption peaks. The decrease in absorption intensity for Fe^{3+} might be due to the fact that Fe^{3+} coordinates by reduced bond order with a long distance with the O atom in the hydroxyl group, causing the previously conjugated system to be deformed by considerable steric hindrance with electrostatic attraction. These findings suggest that PMNOL can act as a metal ion sensor. The all calaulated value is shown in Table 1

Table 1
Observed LOD, LOQ, Binding constant and stoichiometry ratio

S.No.	Metal ion	LOD	LOQ	Binding constant	Stoichiometry Ratio (M : L)
1.	Cu^{2+}	6.7×10^{-6}	20.1×10^{-6}	$0.64 \times 10^{5}\ M^{-1}$	1:1
2.	Fe^{2+}	2.4×10^{-6} M	7.2×10^{-6} M	$0.56 \times 10^{5}\ M^{-1}$	1:1
3.	Fe^{3+}	50×10^{-7} M	16.5×10^{-6}	$0.35 \times 10^{5}\ M^{-1}$	1:2

5. Conclusions

Finally, a new Schiff-base derivative **PMNOL** was synthesized and produced, UV-Vis spectra of it considerably impacted by the type of solvent, pH, concentration and metal cations such as Fe^{2+}, $Fe^{3+,}$ or Cu^{2+} with exceptional selectivity and sensitivity. A peak at 411 nm with a blue shift of 54 nm, 48 nm, and 82 nm are observed for Fe^{2+}, $Fe^{3+,}$ or Cu^{2+} respectively. A isobestic point at about 380 nm is observed for Fe^{2+}, $Fe^{3+,}$ or Cu^{2+} which confirm the formation of complex. As conjugation decreases as formation of complex and electron density shifted at metal so there is blue shift observed. According to Job's

Fig. 4.and colorimetric measurement, the Schiff base ligand binding to metal ions has a 2:1 ligand and metal ratio for Fe^{3+} and 1:1 for Cu^{2+}, Fe^{2+}, and form metal-ligand complexes PMNOL-Cu^{2+}, PMNOL-Fe^{2+} and a 2:1 complex for PMNOL-Fe^{3} this is the first reported Schiff base derivative to the best of our knowledge containing naphthalene and pyridine moieties for colorimetric discrimination of Fe^{2+} from Fe^{3+} along with Cu^{2+}.

Declarations

Ethics approval and consent to participate- Not applicable

Consent for publication Not applicable

Competing interests Not applicable

Funding Not applicable

Authors' contributions CONCEPTUALIZATION, WRITING AND DRAFTING- Poonam Kaswan

Acknowledgements- PK is thankful for AUH, Haryana to provide space for

Authors' information (optional)

Poonam Kaswan, was born in Churu (Rajasthan), India. Poonam Kaswan received her M Tech degree from the Indian Institute of Technology in New Delhi, India. She researched "Transition Metal Complexes of Bi and Tridentate (N, S, O) Donor Ligands in Catalysis and Metal Ion Detection" for her Ph.D. in Chemistry at Amity University, Haryana. She has been teaching at the college education department for six years. Fifteen of her publications have appeared in international journals and conferences.

References

1. Y. Liu, S. Gao, L. Yang, Y. Liu, X. Liang, F. Ye and Y. Fu, *Front. Chem.*, 2020, **8**, 1–13.
2. G. Bartwal, K. Aggarwal and J. M. Khurana, *J Photochem. Photobiol. A Chem.*, 2020, **394**, 112492.
3. A. K. Manna, J. Mondal, K. Rout and G. K. Patra, *J Photochem. Photobiol. A Chem.*, 2018, **367**, 74–82.
4. I. J. Chang, M. G. Choi, Y. A. Jeong, S. H. Lee and S. K. Chang, *Tetrahedron Lett.*, 2017, **58**, 474–477.
5. T. Li, L. Yu, D. Jin, B. Chen, L. Li, L. Chen and Y. Li, *Anal.Methods*, 2013, **5**, 1612–1616.
6. V. Tekuri, S. K. Sahoo and D. R. Trivedi, *Spectrochim. Acta A Mol Biomol Spectrosc.*, 2019, **218**, 19–26.
7. N. Narayanaswamy and T. Govindaraju, *Sens. Actuators B Chem.*, 2012, **161**, 304–310.
8. S. Das, K. Aich, S. Goswami, C. K. Quah and H. K. Fun, *New J Chem.*, 2016, **40**, 6414–6420.
9. Y. Wang, C. Wang, S. Xue, Q. Liang, Z. Li and S. Xu, *RSC Adv.*, 2016, **6**, 6540–6550.

10. M. Akbar Ali and M. T. H. Tarafdar, *J Inorg Nucl. Chem.*, 1977, **39**, 1785–1791.
11. A. Hameed, M. al-Rashida, M. Uroos, S. Abid Ali and K. M. Khan, *Expert Opin Ther Pat.*, 2017, **27**, 63–79.
12. X. Xia, D. Zhang, C. Fan and S. Pu, *Applied Organomet. Chem.*, 2020, **34**, 1–9.
13. A. K. Manna, K. Rout, S. Chowdhury and G. K. Patra, *Photochem. Photobiol. Sci.*, 2019, **18**, 1512–1525.
14. F. Cicekbilek, B. Yilmaz, M. Bayrakci and O. Gezici, *J. Fluoresc.*, 2019, **29**, 1349–1358.
15. M. Hazra, T. Dolai, A. Pandey, S. K. Dey and A. Patra, *J Saudi Chem Soc.*, 2017, 21, 240-7.
16. L. Fan, J. can Qin, C. rui Li and Z. yin Yang, *Spectrochim. Acta A Mol. Biomol. Spectrosc.*, 2019, **218**, 342–347.
17. Q. Bing, L. Wang, D. Li and G. Wang, *Spectrochim. Acta A Mol. Biomol. Spectrosc.*, 2018, **202**, 305–313.
18. R. Azadbakht and H. Keypour, *Spectrochim. Acta A Mol. Biomol. Spectrosc.*, 2012, **85**, 293–297.
19. Y. Hao, W. Chen, L. Wang, B. Zhou, Q. Zang, S. Chen and Y. N. Liu, *Anal. Methods*, 2014, **6**, 2478–2483.
20. A. Kundu, P. S. Hariharan, K. Prabakaran and S. P. Anthony, *Sens. Actuators B Chem.*, 2015, **206**, 524–530.
21. V. K. Gupta, A. K. Singh, M. R. Ganjali, P. Norouzi, F. Faridbod and N. Mergu, *Sens. Actuators B Chem.*, 2013, **182**, 642–651.
22. Z. Aydin, *J. Sci. Technol.*, 2021, **11**, 376–383.
23. T. Hu, J. Cheng, L. Li, Y. Zhan, W. Li, Z. Chang and C. Sun, *Inorganica Chim. Acta*, 2019, **498**, 119131.
24. P. G. Sutariya, H. Soni, S. A. Gandhi, J. Prasad and S. S. Soni, *Sens. Actuators B Chem.*, 2021, **331**, 129417.
25. M. Basak, S. Halder and G. Das, *J. Photochem. Photobiol. A Chem.*, 2021, **414**, 113292.
26. A. Kumar, M. Agarwal and A. K. Singh, *J Organomet. Chem.*, 2008, **693**, 3533–3545.
27. R. R. Crichton, in *Metal Chelation in Medicine*, The Royal Society of Chemistry, 2017, 1–23.
28. G. A. Engwa, P. U. Ferdinand, F. N. Nwalo and M. N. Unachukwu, *Mechanism and Health Effects of Heavy Metal Toxicity in Humans*, 2019, **23**.
29. J. Bilcíkova, V. Fialkova, E. Kovacikova, M. Miskeje, B. Tombarkiewicz and Z. Knazicka, *Contemp. Agric.*, 2018, **67**, 187–195.
30. G. Nageswaran, Y. S. Choudhary and S. Jagannathan, *Spectroscopic Methods for Nanomaterials Characterization*, 2017, **2**, 163–194.
31. V. K. Maurya, R. P. Singh and L. B. Prasad, *Orient. J. Chem.*, 2018, **34**, 100–109.
32. P. Sonthalia, E. McGaw, Y. Show and G. M. Swain, *Analytica Chim. Acta*, 2004, **522**, 35–44.
33. E.I. Ogwo, O.P. Ukaogo, C.S. Egedeuzu, *Sky J. Soil. Sci. Environ. Mgt.*, 2015, 5, 85-90.
34. A. Abbasi and M. Shakir, *New J Chem.*, 2018, **42**, 293–300.

35. B. Das, M. Dolai, A. Ghosh, A. Dhara, A.D. Mahapatra, D. Chattopadhyay, S. Mabhai, A. Jana, S. Dey, A. Misra, *Anal. Methods*, 2021, **13**, 4266-79.
36. T. M. Asha, E. Shiju, C. Keloth and M. R. P. Kurup, *Appl Organomet. Chem.*, 2020, **34**, 1–23.
37. S. Muthusamy, D. Zhu, K. Rajalakshmi, W. Zhu, S. Wang, K. B. Lee and L. Zhao, *ACS Appl. Bio Mater.*, 2021, **4**, 1932–1941.
38. O. Alici and D. Aydin, *J Photochem. Photobiol. A Chem.*, 2021, **404**, 112876.
39. P. W. Cheah, M. P. Heng, H. M. Saad, K. S. Sim and K. W. Tan, *Optical Mater.*, 2021, **114**, 110990.
40. M. L. Passos, M. L. Saraiva, *Measurement,* 2019, **135**, 896-904.
41. F. Pena-pereira, I. Costas-mora, V. Romero and I. Lavilla, Trends Anal. Chem., 2011, **30**, 1637–1648.
42. X. C. Chen, T. Tao, Y. G. Wang, Y. X. Peng, W. Huang and H. F. Qian, *Dalton Trans.*, 2012, **41**, 11107–11115.
43. X. Liu, J. M. Cole and K. S. Low, *J. Phys. Chem. C*, 2013, **117**, 14731–14741.
44. F. Inoue, H. Philipsen, A. Radisic, S. Armini, Y. Civale, S. Shingubara and P. Leunissen, *J. Electrochem. Soc.*, 2012, **159**, D437–D441.
45. A. Klamt, *J. Phys. Chem. C*, 1996, **100**, 3349–3353.
46. W. Samerjai, L. Dankhanob, P. Chotimai, P. Jittangprasert and P. Tongraung, I*ran J Sci Technol Trans A Sci*. 2019, **43**, 451–456.
47. J. Al Anshori, D. Ismalah, A. F. Abror, A. Zainuddin, I. Wiani Hidayat, M. Yusuf, R. Maharani and A. Tatang Hidayat, *RSC Adv.*, 2022, **12**, 2972–2979.
48. S. Mondal, S. K. Manna, S. Pathak, A. Ghosh, P. Datta, D. Mandal and S. Mukhopadhyay, *New J. Chem.*, 2020, **44**, 7954–7961.
49. A. Cihaner and F. Algi, *J. Electroanal. Chem.*, 2008, **614**, 101–106.
50. A. Cihaner, O. Mert, A.S. Demir, *Electrochim. Acta.*, 2009, **54**, 1333-8.
51. S. Gurusamy, K. Krishnaveni, M. Sankarganesh, V. Sathish, P. Thanasekaran and A. Mathavan, *J Mol.Liq.*, 2021, **325**, 115190.
52. X. Zhang, L. Y. Shen, Q. L. Zhang, X. J. Yang, Y. L. Huang, C. Redshaw and H. Xu, *Molecules*, 2021, **26**, 1233.
53. K. J. Gutiérrez, W. M. Pedreira and D. M. Piñero Cruz, *J Coord. Chem.*, 2019, **72**, 2654–2668.
54. B. Tharmalingam, M. Mathivanan and B. Murugesapandian, *Spectrochim Acta A Mol Biomol Spectrosc.*, 2020, **242**, 118749.
55. S. Dhasarathan, , Selvaraj PK. *Turk. J. Chem..* 2022, **46**, 1024-41.
56. S. Ghosh, D. Singharoy, S. Konar, J. P. Naskar and S. C. Bhattacharya, *J Coord. Chem.*, 2021, **74**, 1272–1283.
57. X. Wan, H. Ke, J. Tang and G. Yang, *Talanta*, 2019, **199**, 8–13.
58. X. Wang, Q. Wang, Y. Chen, J. Li, R. Pan, X. Cheng, K. W. Ng, X. Zhu, T. He, J. Cheng, Z. Tang and R. Chen, *Photonics Res.*, 2021, **9**, 213.

59. C. Y. Huang, *Methods Enzymol.*, 1982, **87**, 509–525.
60. R. Ragone and A. Facchiano, *Anal. Biochem.*, 2003, **313,** 170-2.
61. K. C. Ingham, *Anal. Biochem.*, 1975, **68**, 660–663.

Charts And Schemes

Charts 1, 2 and Schemes 1, 2 are available in the Supplementary Files section.

Figures

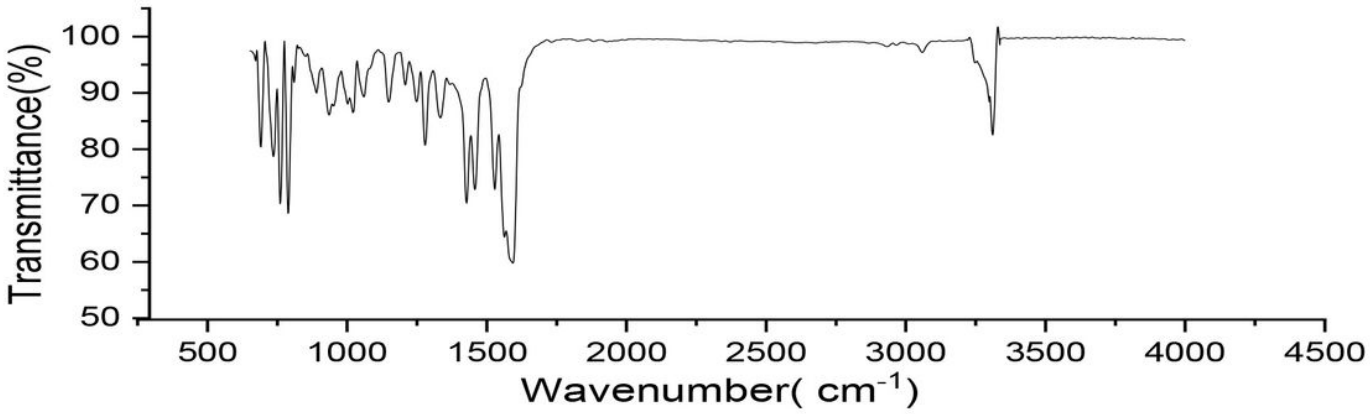

Figure 1

FTIR of 2-(1-(pyridin-2-ylmethylimino)ethyl) naphthalen-1-ol (PMNOL)

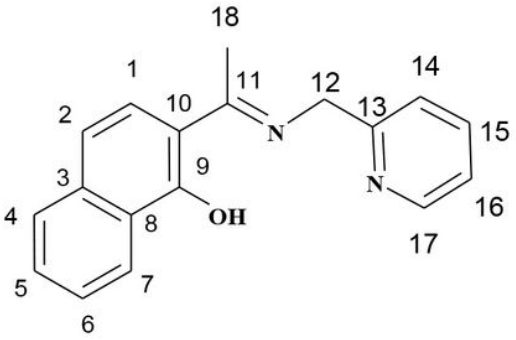

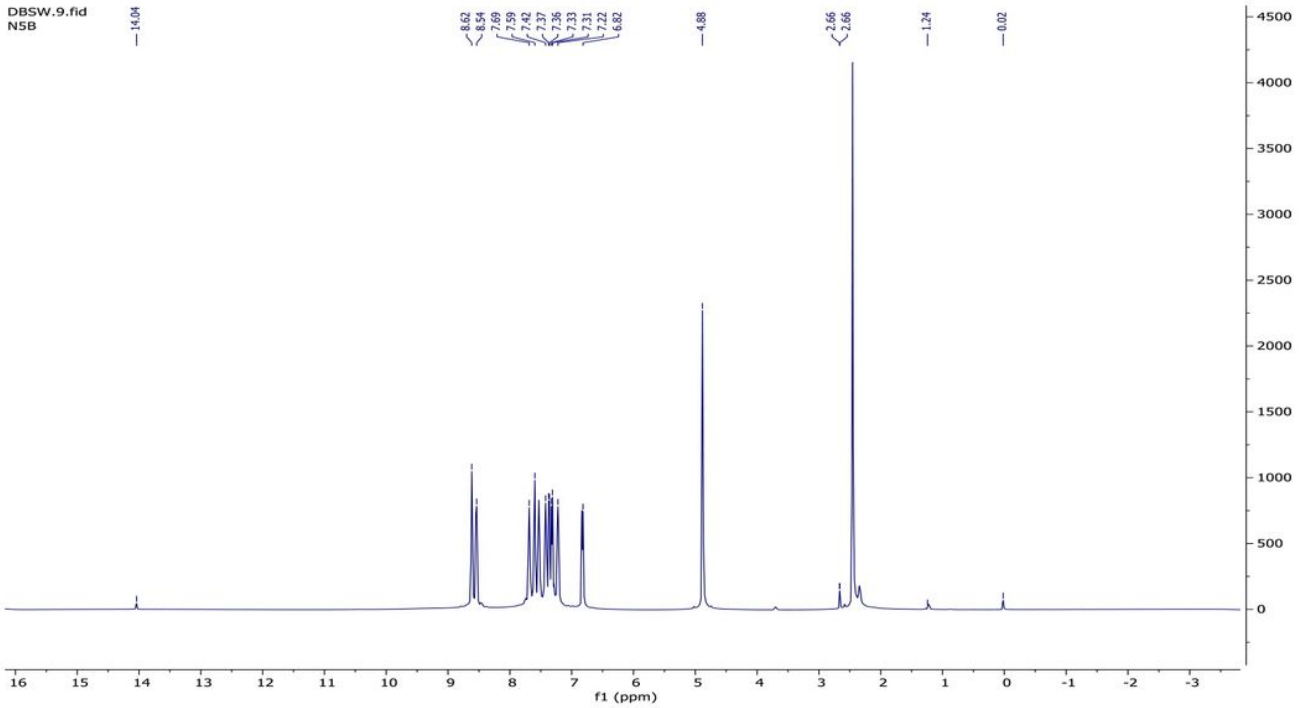

Figure 2

^{1}H NMR of 2-(1-(pyridin-2-ylmethylimino)ethyl)naphthalen-1-ol

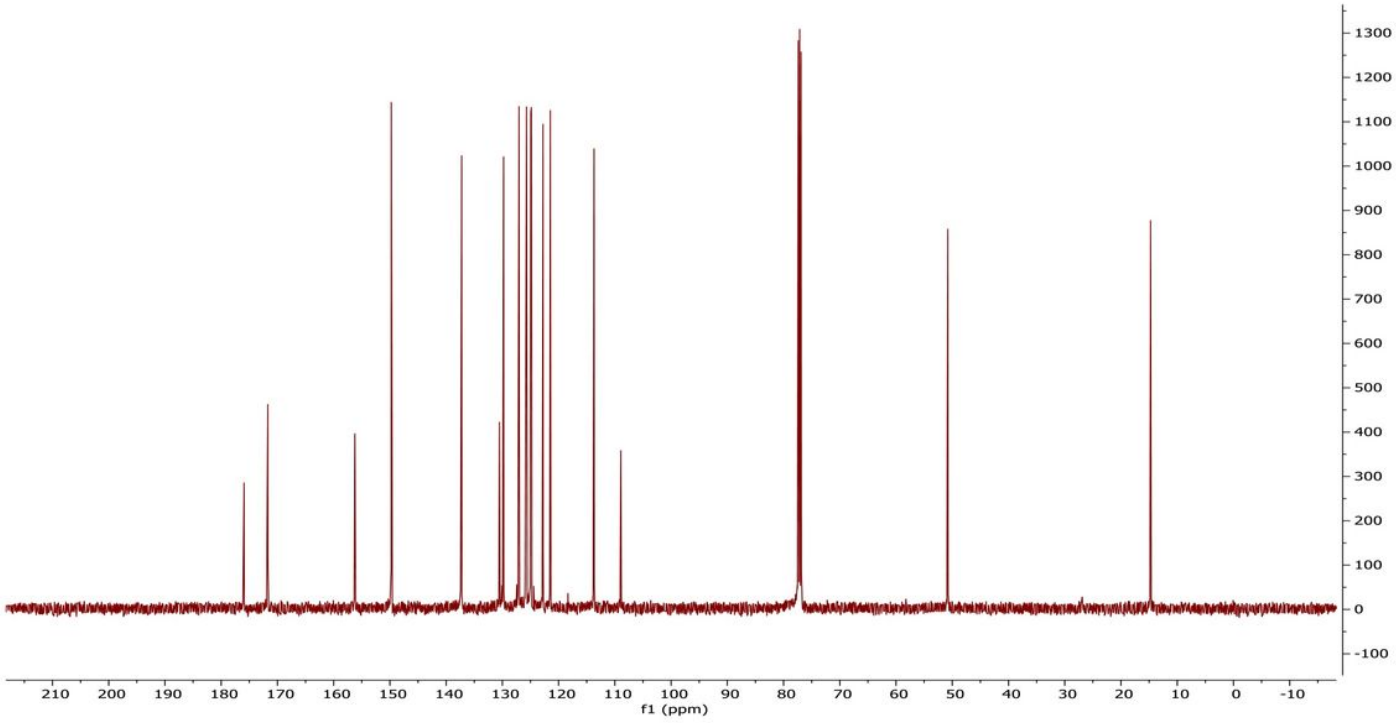

Figure 3

$^{13}C\{^{1}H\}$ NMR of 2-(1-(pyridin-2-ylmethylimino)ethyl)naphthalen-1-ol ligand

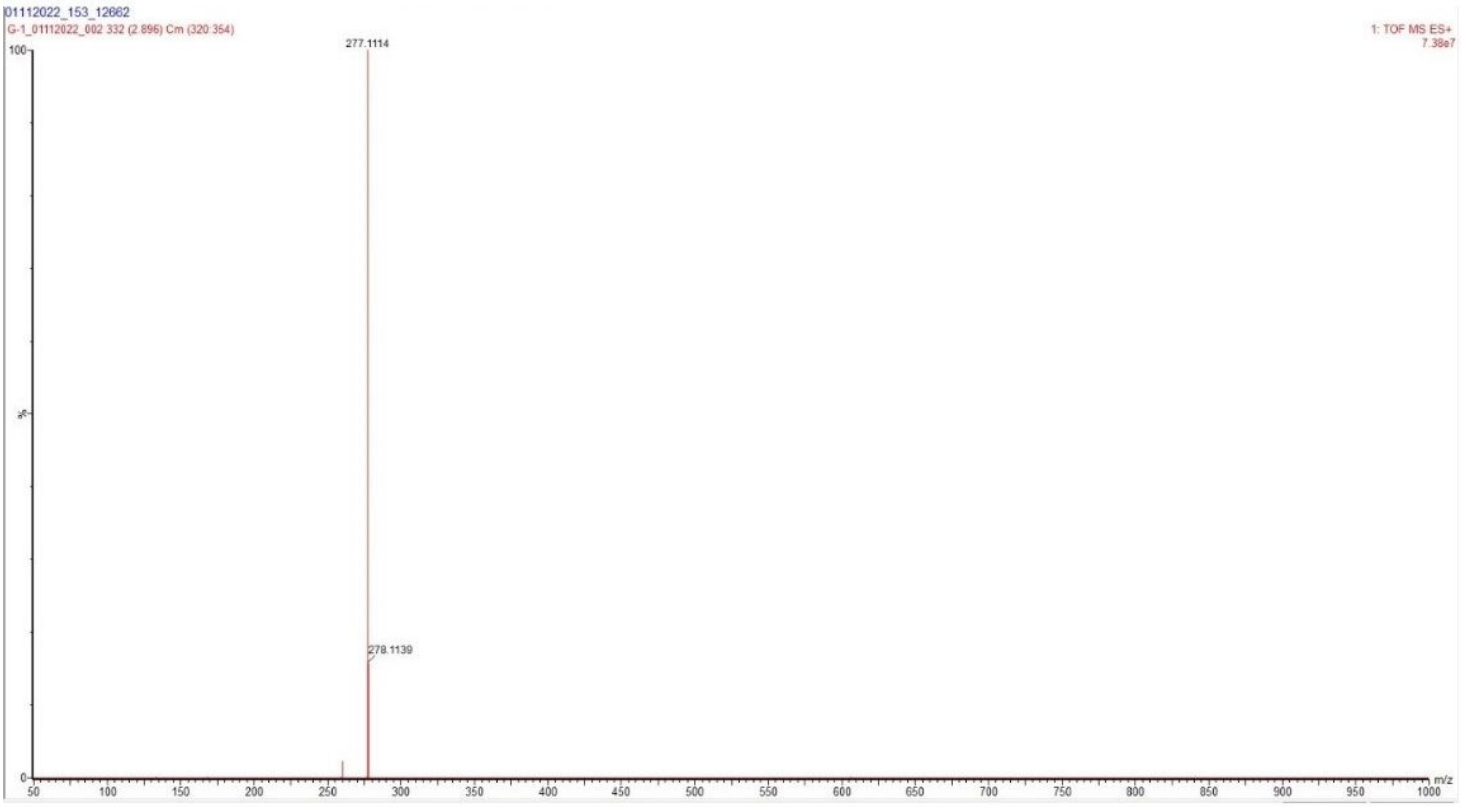

Figure 4

Mass spectra of 2-(1-(pyridin-2-ylmethylimino)ethyl) naphthalen-1-ol (PMNOL)

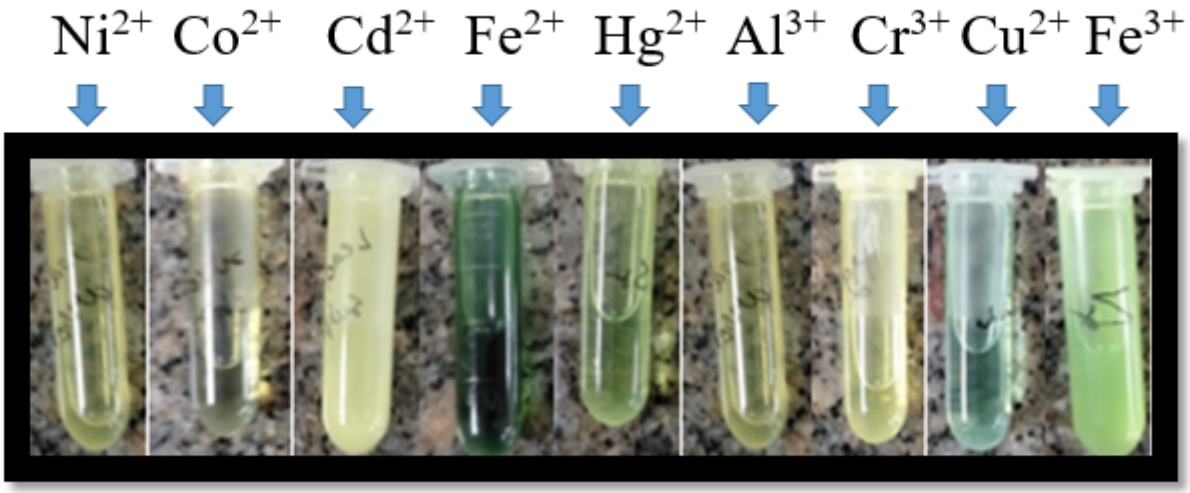

Figure 5

Colorimetry Analysis by the naked eye with different metal ions Ni^{2+}, Co^{2+}, Cu^{2+}, Fe^{2+}, Fe^{3+}, Hg^{2+}, Al^{3+} Cr^{3+}, and Cd^{2+} were prepared with a 5×10^{-2} M and 5×10^{-2} M of PMNOL

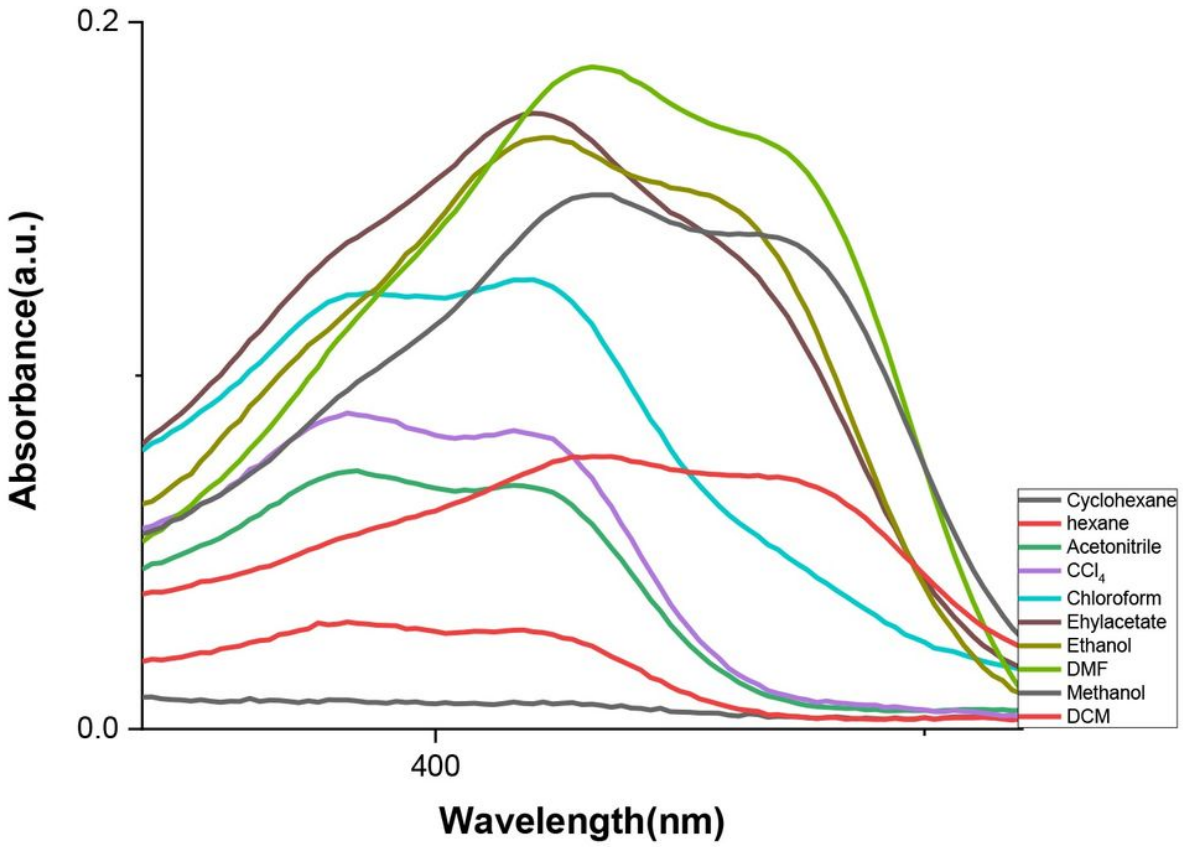

Figure 6

Solvent effect DMF, ethyl acetate, hexane, cyclohexane, ethanol, chloroform, methanol, CCl_4)

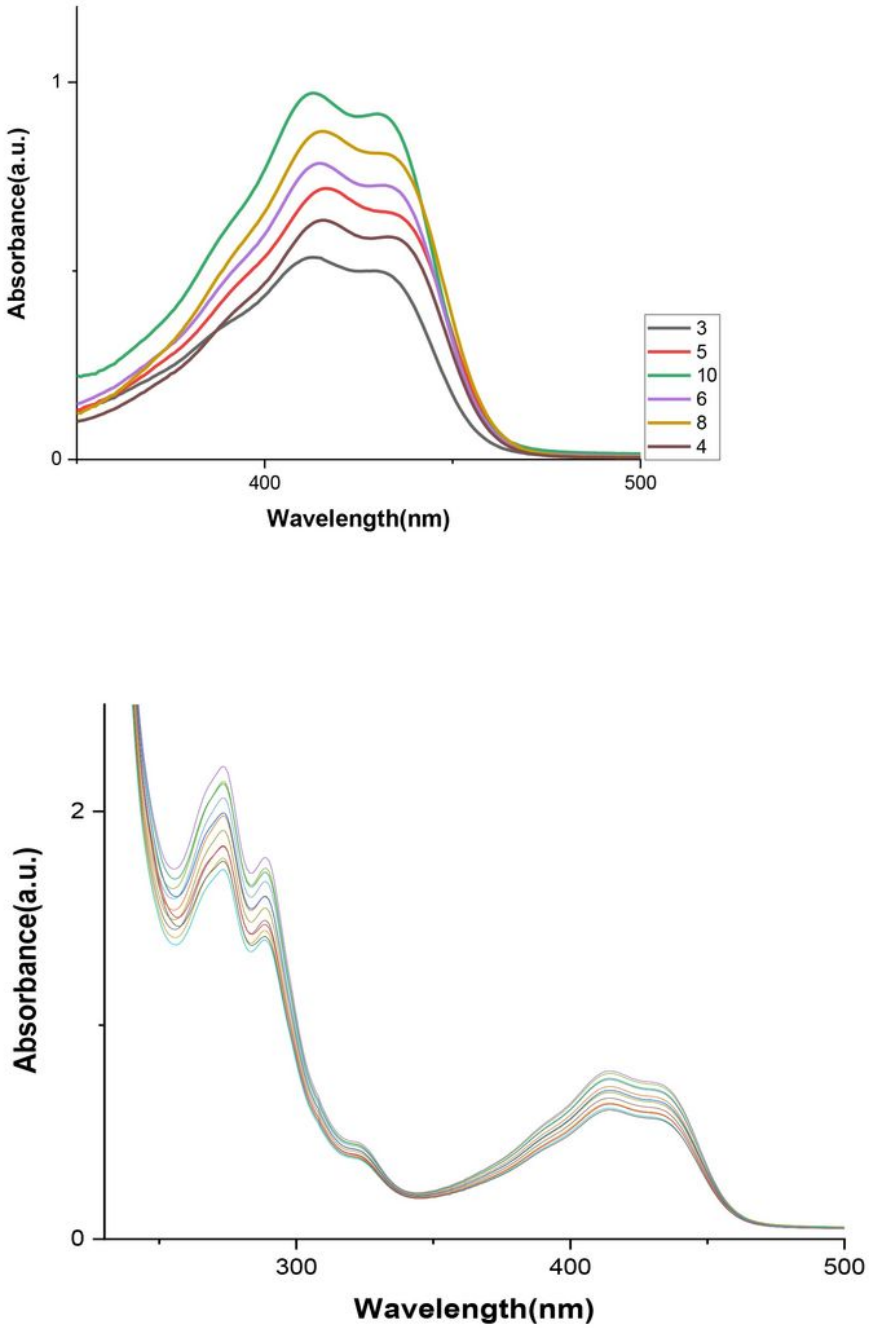

Figure 7

pH effect 3.0, 4.0, 5.0, 6.0, 8.0 and 10.0 and concentration effect.

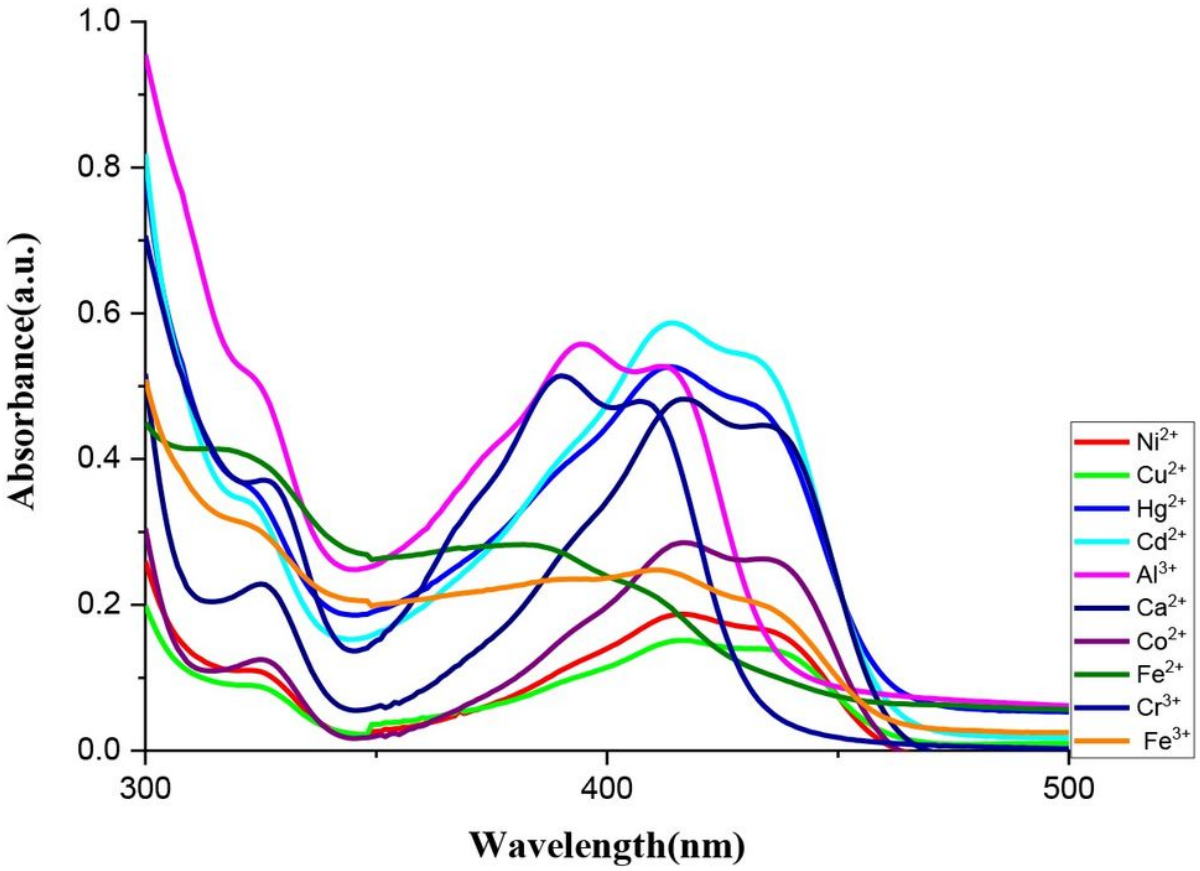

Figure 8

(a) UV–Vis profile for ligand PMNOL(5×10^{-5} M, in DMF) and (b) UV–Vis profile for ligand PMNOL with titrating against a methanolic solution of Ni^{2+}, Co^{2+}, Cu^{2+}, Fe^{2+}, Fe^{3+}, Hg^{2+}, Al^{3+} Cr^{3+}, $Ca^{2+}$and Cd^{2+}

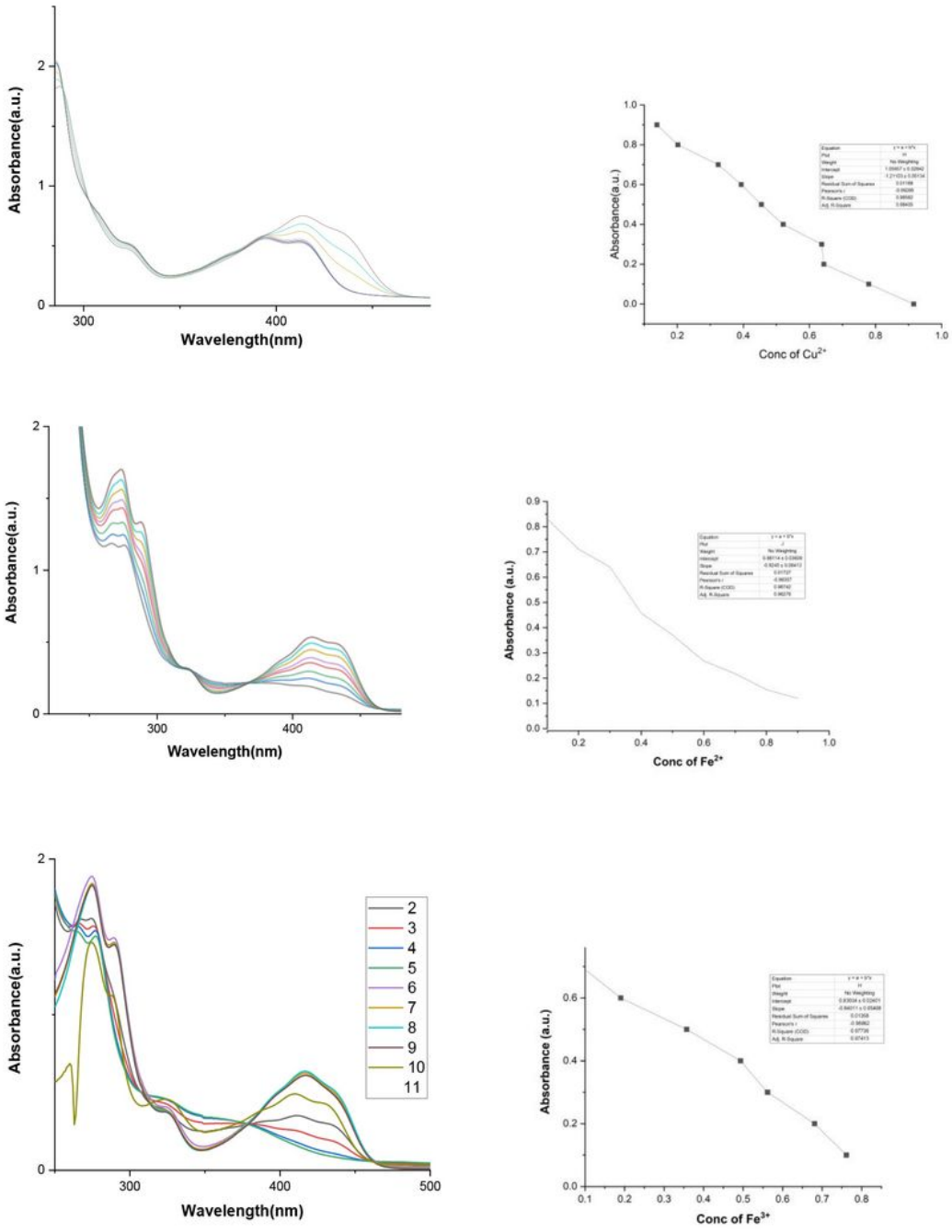

Figure 9

(a) UV-Vis spectra of **PMNOL** (5×10^{-5} M) with an increasing amount of Cu^{2+} (5×10^{-5} M) (b) calibration curve for Cu^{2+} (c) UV-Vis spectra of **PMNOL** (5×10^{-5} M) with increasing amount of Fe^{2+} (5×10^{-5} M) (d) calibration curve for Fe^{2+} (e) UV-Vis spectra of **PMNOL** (5×10^{-5} M) with an increasing amount of Fe^{3+}, (5×10^{-5} M) (f) Calibration curve for Fe^{3+}

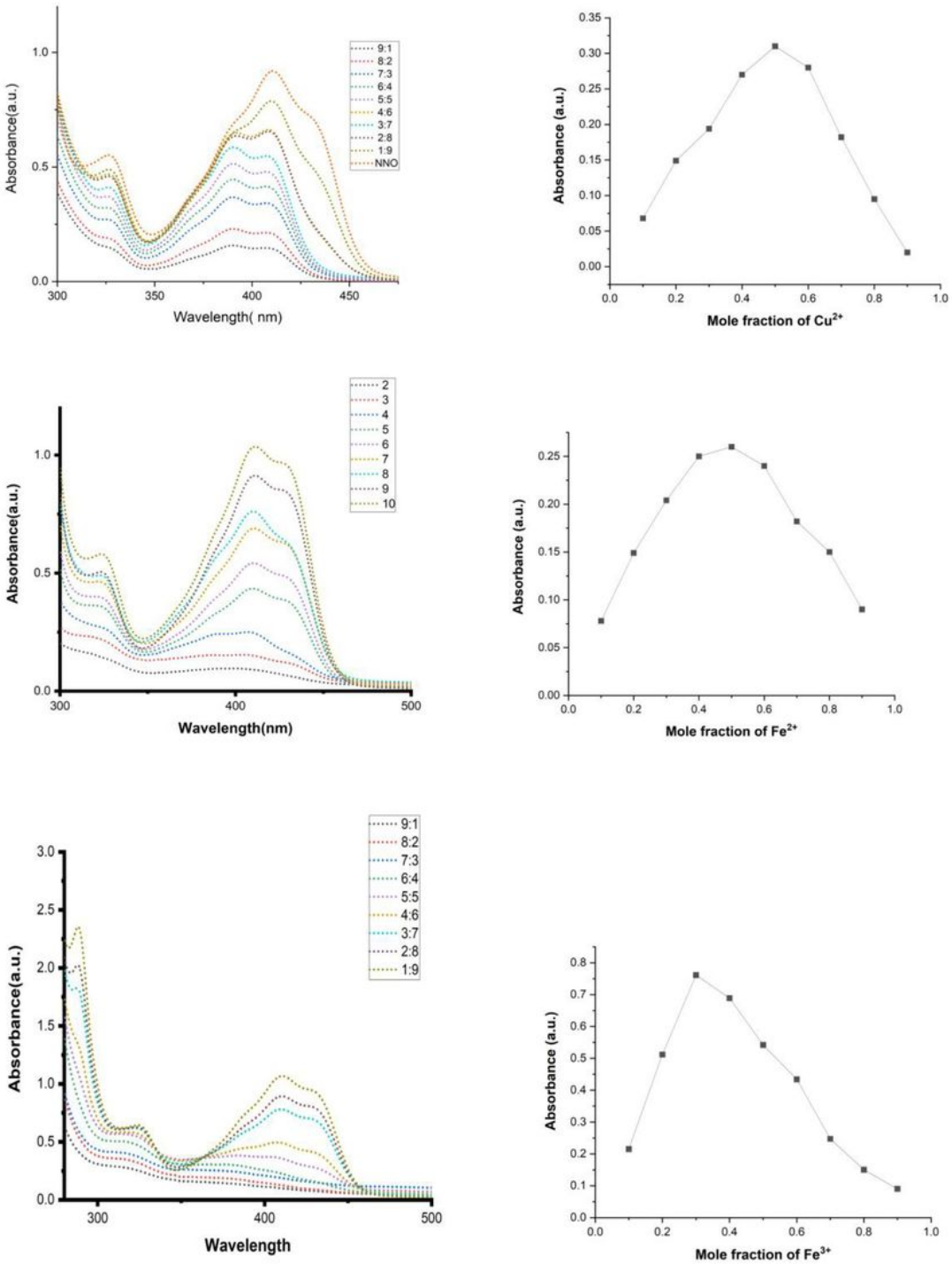

Figure 10

Job's plot for stoichiometry determination between $[A]_0$-[A] and mole fraction of metal ion (0.1,0.2. 0.3, 0.4, 0.5, 0.6, 0.7, 0.8 and 0.9) (a) Cu^{2+} (b) Fe^{2+} (3) Fe^{3+}

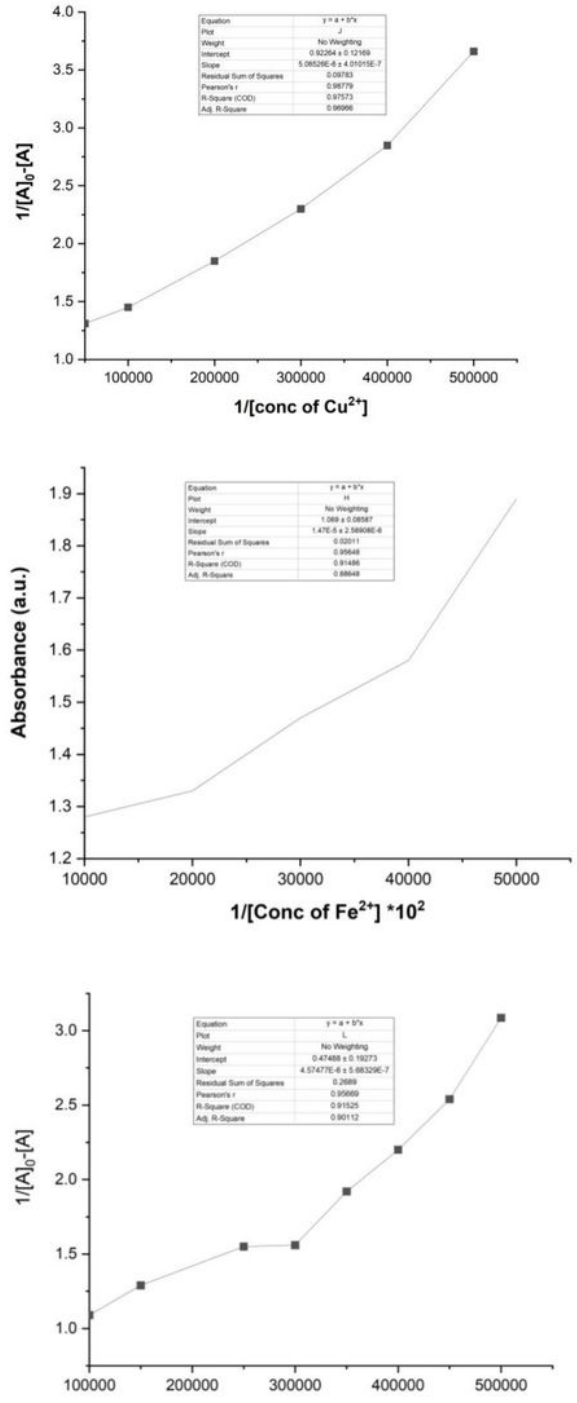

Figure 11

Benesi-Hildebrand plot between $1/[A]_0$-[A] and 1/ [conc. of metal] to determine the binding constant (a) Cu^{2+} (b) Fe^{2+} (3) Fe^{3+}

Supplementary Files

This is a list of supplementary files associated with this preprint. Click to download.

- Graphicalabstrac3.docx
- ChartsandSchemes.docx